Acta Scientiarum
http://periodicos.uem.br/ojs
ISSN on-line: 1807-8664
Doi: 10.4025/actascitechnol.v46i1.66777

Synthesis, morphological characterization, and evaluation of nano zero-valent iron (nZVI) in the degradation of water contaminated with POPs

João Paulo Fortes[1*], Karen Cristina Inácio[2], Alberto Gonçalves Viera de Carvalho Neto[3], Stefany Marques Silva Fortes[4], Renata Ribeiro[5] and Gustavo Henrique Ribeiro da Silva[1]

[1]Programa de Pós-graduação em Engenharia Civil e Ambiental, Faculdade de Engenharia de Bauru, Universidade Estadual Paulista, Bauru, São Paulo, Brazil. [2]Departamento de Química, Faculdade de Ciências de Bauru, Universidade Estadual Paulista, Bauru, São Paulo, Brazil. [3]Programa de Pós-graduação em Ciência e Tecnologia de Materiais, Laboratório de Materiais Supercondutores e Nanoestruturados, Universidade Estadual Paulista, Bauru, São Paulo, Brazil. [4]Centro Universitário Unifio, Ourinhos, São Paulo, Brazil. [5]Programa de Pós-graduação em Biotecnologia, Universidade Federal de São Carlos, São Carlos, São Paulo, Brazil. *Author for correspondence. E-mail:

ABSTRACT. Nanostructured zero valence iron (nZVI) has been applied in advanced oxidative processes aimed at the treatment of water contaminated with Persistent Organic Pollutant (POP). Considering that such compounds cannot be eliminated by traditional treatment methods, this study proposes the synthesis of nZVI by the reduction of Iron Chloride III by sodium borohydride in the absence of O_2, in ultrasound bath. The material obtained has only a wide diffraction halo at 45.13º of 2θ, with an average diameter of the crystallite calculated at 8.3 nm. The method of Brunauer, Emmett and Teller (BET method) analysis infer that the synthesized material is classified as mesoporous and showing a large surface area of 91.48 $m^2.g^{-1}$. According to transmission electron microscopy (TEM) the compound exhibits a core-shell type structure being the average size smaller than 50 nm. Thermogravimetric analysis demonstrates that the compound is thermally stable, exhibiting only a thermal event close to 70º C in which there is a loss of approximately 25% of mass related to water loss. The synthesis was efficient because there is no formation of metal oxides and no residue from the synthesis process according to FT-IR analyzes. To evaluate the effectiveness and present the parameters that most positively contributed to the degradation of water contaminated with 24 of the most common POPs, a chemometric study was applied considering the following variables: reaction time, concentration of applied iron nanoparticles and pH values. The approach reduces costs, time, and waste generation. Among the variables, reaction time is crucial, mainly due to solubility differences between compounds. Kinetic tests show increased efficiency after one hour, emphasizing a direct correlation between degradation rate and water solubility for the studied POPs.

Keywords: Heterogeneous catalysis; POP; nanostructured zero-valent iron; remediation; kinetic tests.

Received on January 22, 2023.
Accepted on January 16, 2024.

Introduction

The world population growth after the 1950s, that went from 2 billion to 7.7 billion in the year 2019, with an increase forecast to 9.2 billion in the year 2050 (United Nations, 2020) made the industry and agroindustry to increase their level of production to supply the growing demand for food. Associated to terrible environmental habits developed by the growing population, an environmental erosion has been witnessed in recent decades with no precedent in history. The increase in the demand for food has forced the agribusiness to use pesticides based on Persistent Organic Pollutants (POPs) (Côrtes, Alves Filho, Ruiz, & Teixeira, 2011), which are not effectively eliminated by traditional treatment systems, especially due to its high toxicity, low biodegradability and biosolubility in lipid tissue (Galassi, Viganò, & Sanna, 1996). For this reason, they represent most pollutants considered a priority by the UNEP (United Nations Environmental Program) and banned or restricted by the Stockholm Convention, May 2001. Methods for soil decontamination with POPs include incineration, desorption, solidification / vitrification, phytoremediation, bioremediation and electrokinetic methods (Terry & Bañuelos, 2020). However, since the costs involved for some of these processes are extremely high, these methods are rarely applied. Advanced oxidative processes are an interesting alternative in the treatment of these contaminants, especially the use of metallic materials has attracted the attention of researchers in the last decade.

The use of metallic materials in remediation procedures consists in the fact that organic compounds can have their oxidation process accelerated due to the presence of metallic compounds in aqueous media, thus causing their degradation (Litchfield, 2005; Srivastava, Srivastava, & Srivastava, 2023). Therefore, when metals oxidize in the presence of organochlorine contaminants, such as trichloroethene or carbon tetrachloride, among others, these organic molecules are captured in the reaction and degraded during the oxidation / reduction process in less toxic organic compounds (Atterby, Smith, Chaudhry, & Stead, 2002). Metallic iron can effectively reduce a wide variety of organic compounds such as chlorinated aliphatics, nitroaromatics, polychlorinated biphenyls (PCBs) (Beyer & Biziuk, 2009; Cundy, Hopkinson, & Whitby, 2008; Kamat & Meisel, 2003; Zhang, 2003) and several pesticides (Côrtes et al., 2011; Xi, Mallavarapu, & Naidu, 2010). Thus, in the present study, an ultrasound bath is used in order to obtain a compound with greater surface area.

This study proposes an improvement in the synthesis parameters in relation to the one proposed by Wang and Zhang (Mamani, Gamarra, & Brito, 2014; Wang & Zhang, 1997), in addition to an extensive characterization presenting several analyzes that support the efficiency of the synthesis method and the benefits of the synthesis occurring in the ultrasound bath, which provides the material with greater surface area and less particle aggregation, being a more interesting alternative to the synthesis method proposed by Wang and Zhang (Sun, Li, Zhang, & Wang, 2007; Wang & Zhang, 1997; Zhang, Nazarian, Wang, & Cranford, 2018). Another point that is fundamental is the study of the potential for POPs degradation by the nZVI synthesized here is the use of gas chromatography to study the degradation of 14 of the most common POPs in aqueous media, analyzing the variables that most favor degradation. The results reported can contribute both to a better understanding of the morphology of nZVI, as well as contribute to optimizing the POPs degradation process.

Material and methods

Synthesis of nanoparticles

A 70% v / v ethyl alcohol solution (Dynamic, P.A) was prepared by bubbling nitrogen gas (N_2, White Martins) for 30 minutes. Subsequently, a 10 mL aliquot was taken in a beaker, and 0.7000 g of sodium borohydride (Aldrich > 98%) was added. The first beaker (beaker A) was then separated. Following, a 10mL aliquot of the 70% v / v ethanol solution was taken again, and 2.7000 g of Iron Chloride III Hexahydrate (Sigma-Aldrich > 98%) was added. The solution was then homogenized until complete dissolution of the salt (Becker B).

Subsequently, the solution contained in beaker A (70% v / v ethanol with sodium borohydride) was transferred to a volumetric flask, then the Becker B content (70% v / v ethanol with iron chloride) was added under the action of the ultrasound bath, dripping 1mL at a time until the entire volume was transferred. The Becker B content was then washed with the Becker A solution and the volume obtained was added to the synthesis medium.

After the reaction time of 15 minutes in an ultrasound bath, the solution was transferred from the volumetric flask to a falcon tube and was centrifuged 3 times with ethanol washing for cleaning, then the solid part was filtered, vacuum filtered, and then dried in the desiccator with N_2 atmosphere.

Characterizations

The thermogravimetric analysis / Differential thermal analysis (TG/DTA) in the present study was performed on a Netzch equipment, model STA 499 F3. The sample was deposited in an alpha-alumina crucible with a volume of 150 µL and a sample mass of 20 mg. The heating rate was 10 ° $C.min^{-1}$ and a dry air flow of $50mL.min^{-1}$ with an interval of 30-600°C.

The X-ray diffractogram (XRD) was obtained using a SHIMADZU XRD 6000 X-ray diffractometer, operating at a resolution of 2 min^{-1} in the 2θ scanning range from 1 to 50º. The analyzes were performed using Cu Kα radiation (λ = 0.15406 nm) and Ni filter under an acceleration of 40 kV and a current of 30 mA.

The textural analysis by adsorption of N_2 at 77K was used in the present study to determine the surface area and to study the distribution and pore characteristics of the pulverized and / or porous materials. The measurements were performed on a Micrometrics equipment, model ASAP 2010.

Regarding FT-IR analyzes, this technique aimed to evaluate the chemical species present in the material. The equipment used for the measurements is of the Bruker brand, model Vertex 70, in which it operated in

the mode of transmittance. The samples were prepared by mixing with KBr (spectroscopic grade) at 1% and pelletized before being subjected to analysis in the medium infrared region (4000 cm^{-1} to 350 cm^{-1}).

The transmission electron microscope (TEM) was used to obtain high resolution images, up to 0.8 Å.

Degradation study

Focusing on planning and optimizing the experimental condition of remediation of POPs with nanostructured zero-valent Iron nanostructures, chemometric analysis was used for variables such as Fe^0 concentration, time, and pH value in the experiment. For that, a 2^{3-1} fractional factorial experiment was used, with the execution of 4 experiments, half of what would be necessary for a complete factorial design of 2^3. The experiment matrix was obtained using the trial version of the Design Expert software version 11 and the variables studied in the present study are presented on Table 1.

Table 1. Conditions analyzed in fractional factorial design (2^{3-1}) for remediation studies of aqueous samples contaminated with POPs using nanostructured iron.

Test	pH	Time (min)	Amount of added nanoparticle (μg mL^{-1})	Concentration of POPs (μg mL^{-1})
1	3	90	400.0	4.0
2	10	90	200.0	4.0
3	3	180	200.0	4.0
4	10	180	400.0	4.0

It is worth mentioning that the application of nanoparticles in the remediation process was carried out with dry samples, thus justifying that the mass values of nanoparticles applied in remediation already consider the loss of water mass.

Results and discussion

Thermal analysis (TGA/DTA)

The thermal analysis (TGA/DTA) of the obtained materials was used to verify if, after the synthesis of the nanoparticles, traces of the reagents remain, as well as to verify the thermal behavior of the material.

On the thermogravimetric curve (Figure 1) it is possible to notice, a 25.73% of mass loss was noticed, possibly traces of water from the 70% v/v ethanol solution used in the synthesis and subsequent washing of the material. Contrasting with the curve referring to the DTA (μV / mg^{-1}) which indicates the thermal events of the material used in the synthesis, an endothermic peak adjacent to the place where the curve of mass loss stabilizes is observed, indicating that the compound has reached stability in terms of mass loss. Similar behavior was observed by Baikousi (Baikousi et al., 2015), in which a loss of approximately 15% of the sample obtained in the same temperature range was evidenced by the same synthesis process.

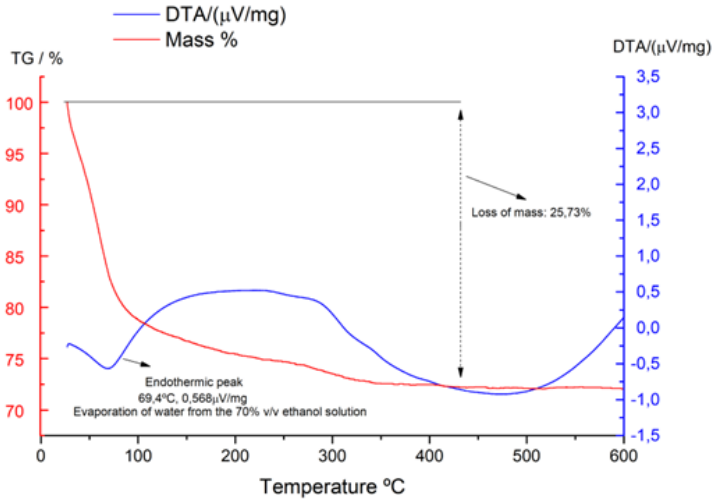

Figure 1. DTA curve referring to the nanostructured zero-valence iron sample.

Structural characterization by X-Ray Diffraction (XRD)

Through the diffractogram shown in Figure 2, as described by Taha and Ibrahim (Taha & Ibrahim, 2014) it is possible to notice a wide diffraction halo in 45.13° of 2θ which is a confirmation of zero valence iron. It is also possible to estimate the size of the crystallite according to the Scherrer equation at 8.3 nm (Huggins, 1945). In view of the absence of diffraction halos at 62.1° of 2θ and smaller halos around 30º and 35º of 2θ, it is possible to infer that the methodology employed (both the use of an alcoholic medium and the absence of O_2) prevented oxidation of the material, avoiding the formation of iron oxide (Wang & Zhang, 1997; Xi et al., 2010; Zhang, 2003). Such minor halos (referring to Iron II oxide) were found by Sun (Sun, Li, Cao, Zhang, & Wang, 2006), considering that Sun and Zhang did not use N_2 (gas used in this study for O_2 elimination) in his method, it becomes greater evidence that the present method in the absence of O_2 is effective in preventing the sample oxidation process. It is also possible to verify that ethanol not only helps to prevent oxidation, but because it has a lower polarity than water it is also able to stabilize nanoparticles during synthesis.

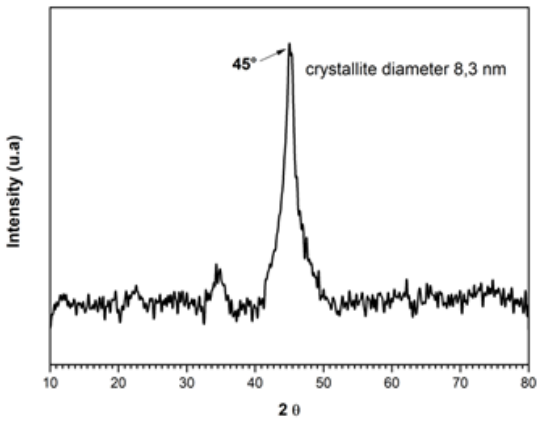

Figure 2. Diffractogram of the sample of metallic iron synthesized in alcoholic medium.

Textural analysis by N_2 adsorption

Figure 3 shows the N_2 adsorption isotherms in the STP on the nZVI sample.

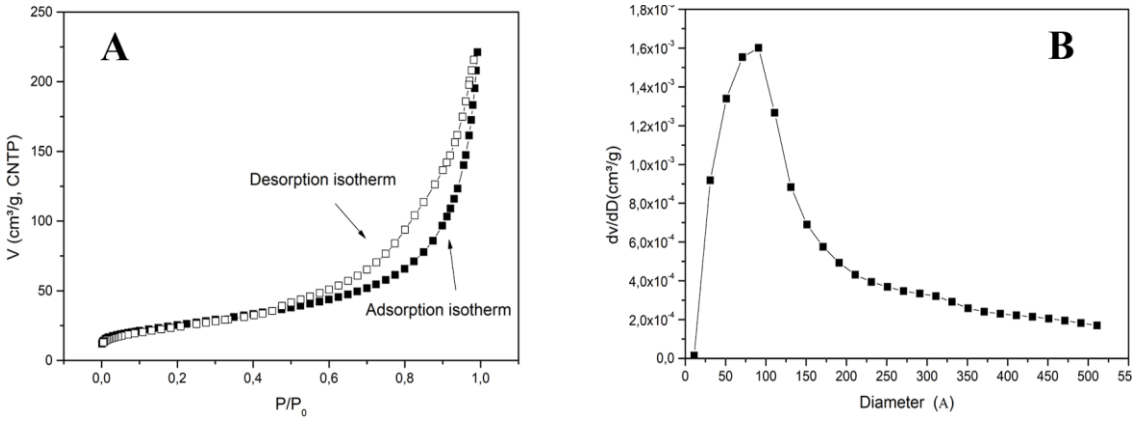

Figure 3. (A) Isotherms of the nanostructured zero valence iron sample without thermal treatment. (Full markers: adsorption branch and open markers: desorption branch). (B) Distribution of pores in samples without heat treatment as a function of the reaction time in alcohol.

As can be seen in Figure 3(A), the isotherms of the nZVI sample are classified as type II on the Brunauer scale (Brunauer, Emmett & Teller, 1938) and are considered the most common types in adsorption models, commonly occurring in non-porous or with pores in the mesoporous range (porous material whose pores have a diameter between 2.5 to 100 nm as also observed by Taha and Ibrahim (Taha & Ibrahim, 2014). These data substantiate those already presented in the discussion of the Scherrer equation, which suggests an average diameter of crystallites at 8.3 nm.

In the entire range of relative pressure, the volume of N_2 adsorbed and the total volume (in P / P0≈1) increased as the reaction time increased, indicating that the reaction increases the porosity of the material and, therefore, the surface area.

Figure 3(B) allows to observe, through the Barret, Joyner and Halenda method (BJH method), the distribution of the average pore size of the samples in relation to dV / dD as a function of the diameter of the pores.

Through the BET analysis it is possible to conclude that the compound has a high surface area (91.48 m^2 g^{-1}), whose majority of the pores presented an average diameter of 8.5 nm, showing a significant improvement using the method presented by Taha and Ibrahim at 6.18 nm. The surface area found in the present study is 161% larger than that presented by Sun (Sun et al, 2006) where the sample was synthesized by the same method. The significant improvement related to the increase in the surface area can be attributed to the dispersion of the particles generated by the cavitation derived from the ultrasonic wave. It prevents the particles from agglomerating thus decreasing the surface area. Similar behavior was described by Esmaeili (Esmaeili & Entezari, 2014) during the graphene oxide synthesis process using a graphene reduction method. Another important factor is that the hysteresis characteristics in the relative pressure range are similar to those of Type H3. Materials that present their pores in the shape of wedges, cones and / or parallel plates, validates the MET analysis of the present study.

Transmission Electron Microscopy (TEM)

TEM was used to evaluate the morphology of the material obtained. In Figure 4, it can be seen the structures, showing that the individual particles are much below the 100 nm scale proposed by the analysis, forming a cluster of crystallites with uniform size. Thus, corroborating with the BET analyses which found that the compound fits as mesopores (particles between 2.5 to 100 nm).

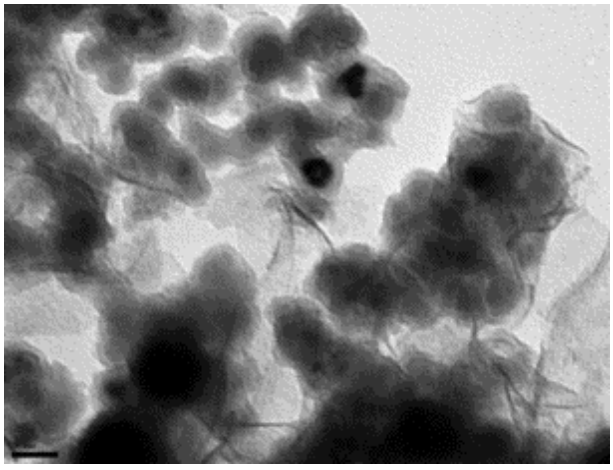

Figure 4. Transmission electron microscopy (MET) on a 20 nm scale for the nanostructured zero-valence iron sample.

The study of the Figure 4 allows the conclusion that the prepared compound presents a broadly spherical aspect characteristic of particles synthesized in solution (Sun et al., 2006), which corroborates with the BET analyses in relation to the H3 type hysteresis format. The TEM images, shown in Figure 4, clearly show the presence of less dense and lighter regions and denser and dark regions for nZVI particles. The darker color represents the core, while the lighter color represents the nanostructured zero-valence iron shell (Taha & Ibrahim, 2014). These results were also found in studies by Li (Li, Elliott, & Zhang, 2006), Sun (Sun et al., 2006) and Baiakousi (Baikousi et al., 2015), and more recently by Taha and Ibraim (Taha & Ibrahim, 2014) who suggest a core-shell structure for nZVI. A determining point observed in the TEM images is that the compound presents greater spacing between the crystallites not found in other studies, possibly due to the synthesis in an ultrasound bath whose agitation may have influenced the state of aggregation of the material. An important aspect to mention is that the hysteresis observed in Figure 3 is not due to the pores of the particle itself, but because of the cavities formed by the agglomeration of particles, as shown in Figure 4. It is also inferred, through the analysis of TEM images, that the average particle size is always smaller than 50 nm, being smaller than the average size observed by Sun (Sun et al., 2006) of 70.2 nm.

Infrared Vibrational Spectroscopy (FT-IR)

To verify possible remnants of sodium borohydride reducer in the final sample, an FT-IR analysis was performed only for the reagent in question, as shown in Figure 5. Although it is a pioneer concern of this study, evaluating the quality of the washing process safeguards a cleaner surface for the nanostructures, guaranteeing maximum contact

of the nanoparticles with the pollutant to be remedied once the residues of reagents on the surface of the material can reduce the effectiveness in the remediation given that, the particle can oxidize the nanoparticles before the POPs. It might even act as a stereo deterrent, preventing POPs from interacting with nanoparticles.

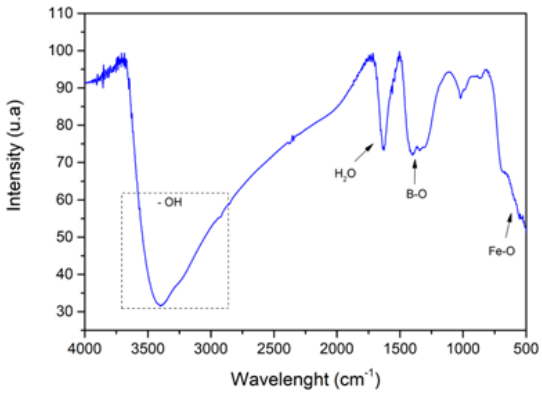

Figure 5. FT-IR spectra for nanostructured zero-valence iron sample.

Figure 5 shows the spectrum of the mid-infrared region (between 4000 and 400 cm^{-1}), of iron as synthesized and without prior heat treatment. Clearly, some of the vibrations detected in the samples could only be observed since the samples were not exposed to heat treatments, such as those associated with the stretching of the OH bond of the solid and wastewater, detected at 3447-3392 cm^{-1} and stretching H_2O at 1620-1670 cm^{-1}. It is also observed a band around 1350 cm^{-1} referring to the stretching of B-O, coming from the sodium borohydride reducer used in the process of synthesis of nanoparticles. It is also observed the formation of a band close to 670 cm^{-1} characteristic of Iron oxide (Fe-O stretch) resulting from the surface oxidation of the compound, corroborating the results presented in the TEM analysis pointing to iron oxide as the shell of the nanoparticles. The analyzed data agree with the ones found by Baikousi (Baikousi et al., 2015) who also synthesized nZVI through the reduction of Fe^{+3} with borohydride.

Degradation study

A chemometric study was carried out to evaluate the efficiency of the nanoparticles synthesized and to understand the factors that most contributed to the degradation of the POPs studied. The variables used can be seen in Table 1. The degradation process was carried out through gas chromatography, with an Agilent 7890A equipment, working in conjunction with an Agilent 5975C Mass Spectrometer.

When evaluating the graphs presented in Figure 6, it can be concluded that test 4 presents the best degradation results once it makes use of the variables at their highest values to obtain the most complete picture of the effect of the variables studied on the degradation process of the POPs studied.

From the data presented in Table 2, it is inferred that the pH value appears as the most relevant factor in the degradation of α-endosulfan, β-endosulfan (improved degradation at pH 10). The time variable is the second most relevant variable, and the concentration of nanoparticles represents the least relevant variable for the remediation process. A similar result was found by Cong (Cong, Guo, Liu, Shi, & Wang, 2015) who reached a degradation value of 90% for endosulfan and its isomers in the same pH and time range, but with the use of zero valence zinc. As identified by Cong himself (Cong et al., 2015), zero valence zinc is much more efficient in the degradation of endosulfan (50% on average using Fe).

Regarding the endosulfan sulfate data, the time variable is shown to be the most relevant for the degradation efficiency, its pH is variable and has the concentration of nanoparticles added. The solubility of the POPs studied may be directly related to the importance of the time variable in the degradation efficiency (The solubilities of α-endosulfan, β-endosulfan and endosulfan sulfate in water are respectively 1.73 mg L^{-1}, 1.16 mg L^{-1} and 0.1025 mg L^{-1}).

The γ-BHC and δ-BHC compounds show a decreasing relationship of importance of variables as follows: nanoparticle concentration proves to be more significant than the reaction time, which ultimately proves to be more significant than the pH value. All variables have positive effects on the degradation process. The β-BHC compound presents itself differently, being the most relevant variable in the contaminant degradation process. Similar behavior presented with the endosulfan isomers, which is also justified by the fact that β-BHC (solubility 0.542 mg L^{-1}) has drastically lower solubility than the other γ-BHC isomers (5.75 mg L^{-1}) and δ-BHC (2.59 mg L^{-1}).

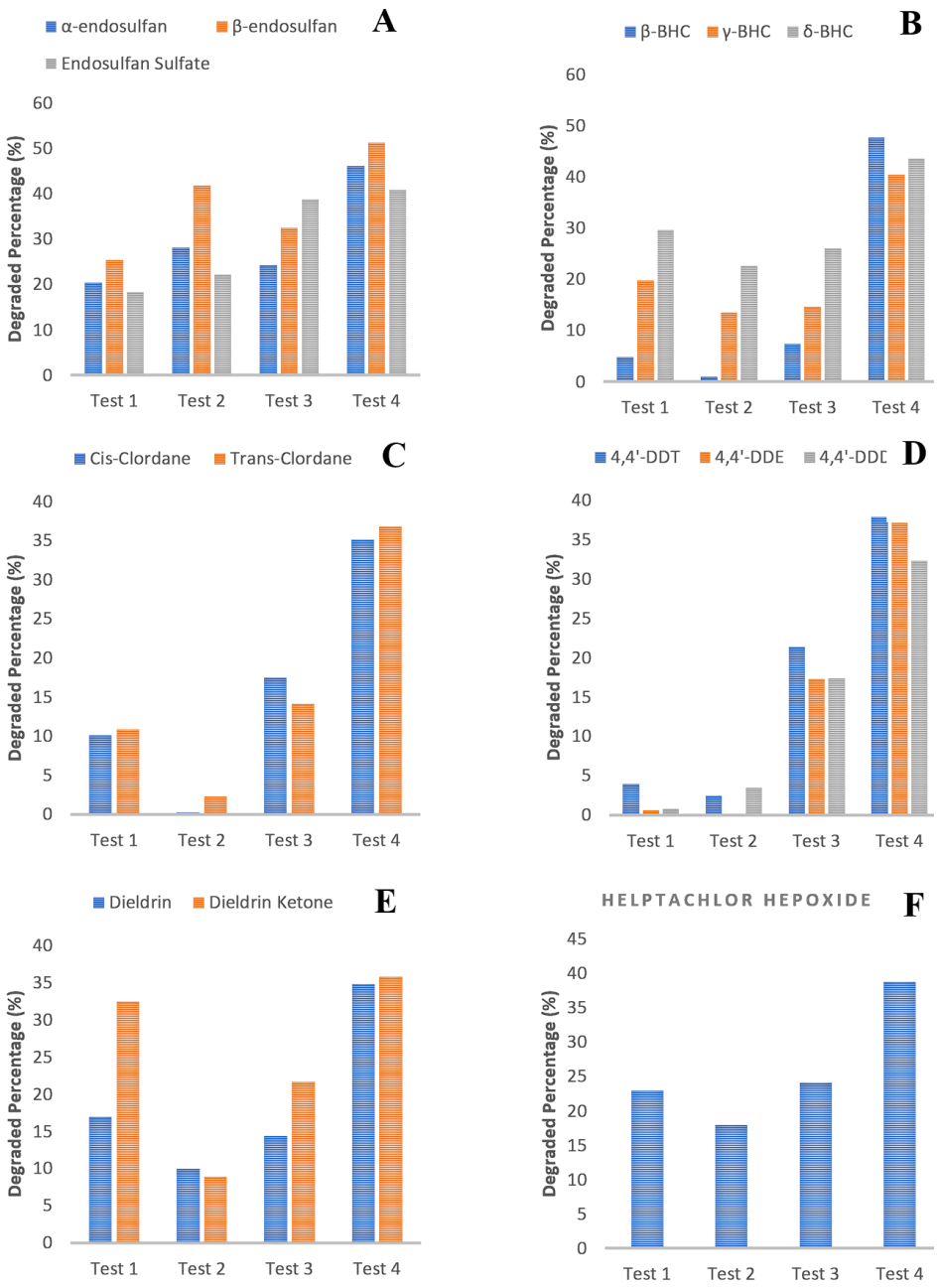

Figure 6. % degradation for compounds (A) alpha-endosulfan, beta-endosulfan and endosulfan sulfate (B) alpha-BHC, gamma-BHC and sigma-BHC (C) cis-chlordane and trans-chlordane (D) o 4, 4'-DDT and its primary metabolites 4,4'-DDE and 4,4'-DDD (E) Dieldrin and Endrin ketone (F) Heptachlor epoxide.

Regarding the degradation of Cis-chlordane and Trans-chlordane compounds. It is possible to observe that the time variable is the most significant in the degradation process, immediately followed by the concentration of nanoparticles, with the pH value being the least significant variable. All of them presenting a positive factor for the degradation of the pollutants in question. Once again, it is noted that compounds with low solubility such as cis-chlordane (0.0464 mg L^{-1}) and trans-chlordane (0.056 mg L^{-1}) present difficulties to interact with the iron nanoparticles that are dispersed in aqueous solution. The compounds 4,4'-DDT and 4,4'-DDE present the time variable as the most significant, followed by the concentration of nanoparticles, and finally the pH value. Although the time factor was also the most important for the 4,4'-DDD compounds, the order of importance was different for this compound, with the pH value being the second most important variable in the degradation factor. The time factor appears to be the variable that has the greatest significance because these compounds are those with the lowest solubility among all the POPs studied (0.0031 mg L^{-1}, 0.065mg L^{-1} and 0.09mg L^{-1}, respectively). The present study points to an average degradation of 35% for DDT and its metabolites with a reaction time of 3 hours, and excess of iron nanoparticles, considering that such compounds have a half-life between 5 and 7 years.

Table 2. Effect ratio of the variables analyzed in the degradation process of Endrin ketone.

		Constant	pH	Time (min.)	Nanoparticle concentration(μg.mL^{-1})
α-ENDOSULFAN	Effect	-	14.780	10.900	7.150
	Coefficient	29.705	7.390	5.450	3.575
β -ENDOSULFAN	Effect	-	176.050	82.550	12.250
	Coefficient	377.575	88.025	41.275	0.6125
ENDOSULFAN SULFATE	Effect	-	176.050	82.550	12.250
	Coefficient	377.575	88.025	41.275	0.6125
β -BHC	Effect	-	10.130	16.540	14.090
	Coefficient	11.150	5.065	8.270	7.045
γ -BHC	Effect	-	9.860	10.890	16.030
	Coefficient	22.080	4.930	5.445	8.015
δ -BHC	Effect	-	5.280	8.640	12.270
	Coefficient	30.455	2.640	4.320	6.135
CIS-CLORDANE	Effect	-	3.875	21.145	13.815
	Coefficient	15.733	1.937	10.572	6.908
TRANS-CLORDANE	Effect	-	7.025	18.875	15.645
	Coefficient	16.038	3.513	9.437	7.823
4,4'-DDT	Effect	-	7.450	26.400	8.980
	Coefficient	16.385	3.725	13.200	4.490
4,4'-DDE	Effect	-	9.695	26.765	10.155
	Coefficient	13.783	4.848	13.382	5.078
4,4'-DDD	Effect	-	8.770	22.670	6.130
	Coefficient	13.465	4.385	11.335	3.065
DIELDRIN	Effect	-	6.750	11.100	13.690
	Coefficient	19.020	3.375	5.550	6.845
ENDRIN KETONE	Effect	-	-4.680	8.090	18.860
	Coefficient	24.665	-2.340	4.045	9.430
HEPTACHLOR HEPOXIDE	Effect	-	6.750	11.100	13.690
	Coefficient	19.020	3.375	5.550	6.845

Regarding the degradation of Dieldrin and Endrin Ketone, firstly, the concentration of nanoparticles stands out as the most significant variable for the degradation of compounds, secondly the time variable and finally the pH value. As for the negative effect of the pH value for the compound Endrin ketone, it shows that it presents a greater degradation at lower pH. A possible explanation for this effect has already been observed in other studies (Nie, Esopi, Janik, & Asthagiri, 2013; Yin et al., 2012) showing that under low pH conditions there is an increase in dehalogenation reaction rates, which is justified by the increase in the concentration of H+ in the solution. However, at higher pH values there is a decrease in the activity of the iron nanoparticle related to the presence of OH- which facilitates the adhesion of Fe(II) and Fe(III) oxides on the metallic surface. In relation to the compound Heptachlor epoxide, which shows the relationship of the effect of variables on the degradation process of Heptachlor epoxide, time is the most significant factor, followed by the concentration of nanoparticles and finally the pH value. Contrasting from the compounds of the Endrin family, all the variables have a positive effect on the degradation of the compound. According to Figure 6(B) the method showed a degradation of 38%, which seems to be a small number, but when considering the half-life of approximately 3 years of the compound in question, the number becomes motivating.

Regarding Figure 7(A) it is noted that the process becomes more effective after one hour of reaction, with an even longer delay for the endosulfan sulfate compound, probably due to the lower solubility of this compound in aqueous media. Figure 7(B) shows once again the difference in solubility between the three compounds presented. The β-BHC isomer is more difficult to degrade. Differently from what was analyzed in the previous figures, Figure 7(C) shows that the cis-chlordane and trans-chlordane isomers present the same behavior, with very similar degradation rates while the kinetic study of heptachlor epoxide shows a slow onset, and after 4 hours of reaction the process increased considerably. In Figure 7(D) it is inferred that the compounds 4,4'-DDE and 4,4'-DDD showed a slightly lower degradation rate compared to the compound 4,4'-DDT and in Figure 7(E) both the Endrin ketone when the Dieldrin showed similar behavior in relation to degradation, and the result after 5 hours of reaction was the same.

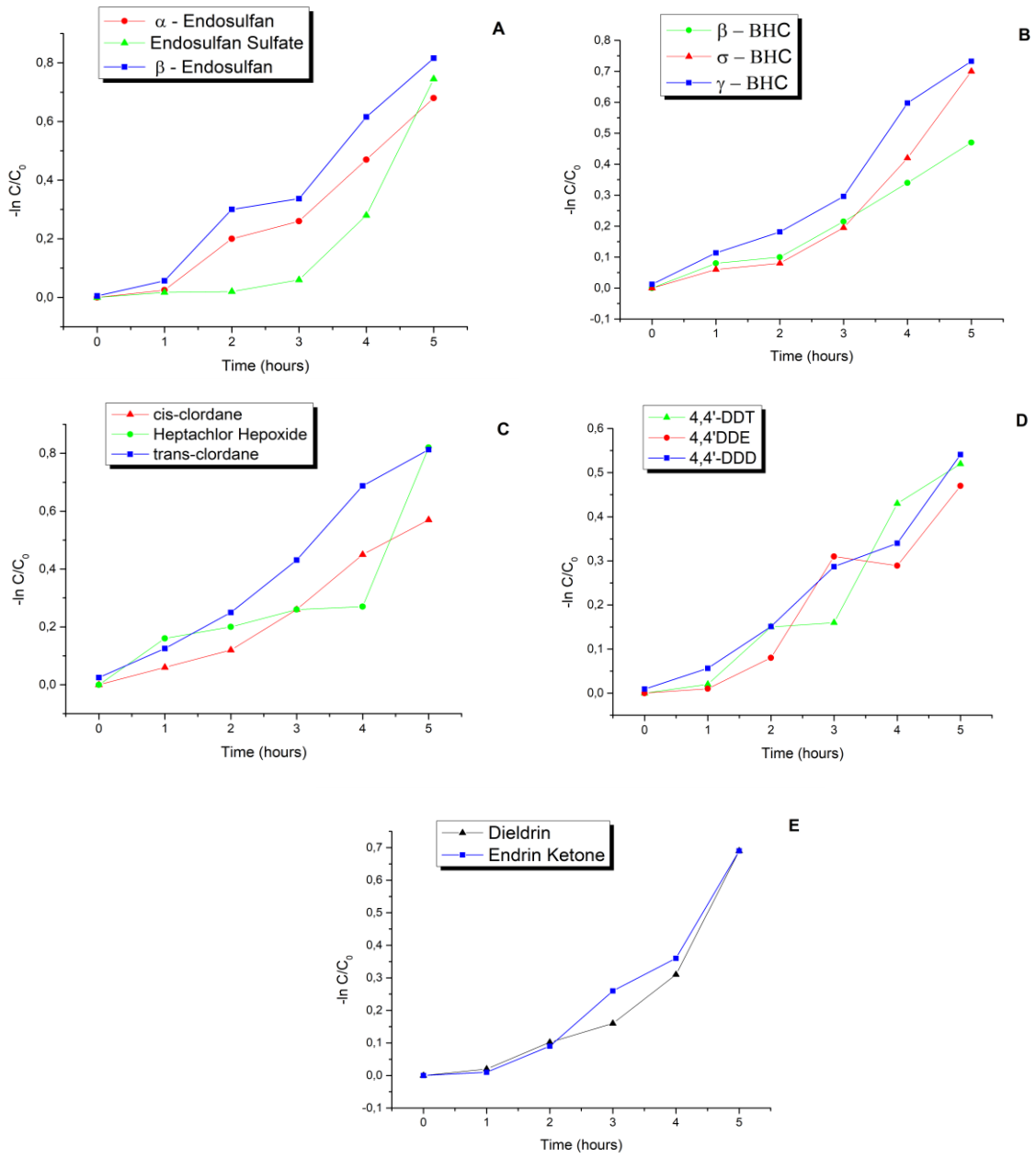

Figure 7. Kinetic study for compounds (A) alpha-endosulfan, beta-endosulfan and endosulfan sulfate (B) alpha-BHC, gamma-BHC and sigma-BHC (C) cis-chlordane and trans-chlordane and Heptachlor Hepoxide (D) o 4 ,4'-DDT and its primary metabolites 4,4'-DDE and 4,4'-DDD (E) Dieldrin and Endrin ketone.

Conclusion

The synthesis process in alcohol medium with borohydride, in the absence of O_2 and in an ultrasound bath, proved to be extremely efficient in the synthesis of nZVI, avoiding the formation of iron oxide, as well as the washing process is also satisfactory for there is no trace of undesirable reagents in the final product. The compound reaches constant mass after 69.4 ° C due to water and alcohol loss. XRD analysis showed that there was only one broad diffraction halo at 45.13° in 2θ and the Scherrer equation infers that the mean diameter of the crystallites is 8.3 nm. Through the BET analysis, it is concluded that the nanostructures are always smaller than 50 nm, corroborating with the TEM analysis, and with the average pore size of 8.5 nm and a high surface area of 91.48 m^2. g^{-1}. In conclusion, the ultrasound bath synthesis process is satisfactory in the synthesis of zero-valued iron nanostructures with high surface area.

Better application conditions could be defined by the chemometric analysis applied to POPs. This technique provided a reduction of costs, time and mainly of generated residues. The three variables affected

the degradation efficiency; however, the reaction time is more important in the degradation process, largely due to the solubility variation that exists between the compounds. In the three POPs studied, kinetic tests showed that the process becomes more efficient after one hour of reaction time. The study suggests that the rate of degradation for the POPs studied is directly related to their solubility in water.

Acknowledgements

The authors would like to thank the postgraduate program in civil and environmental engineering at the Faculty of Engineering of Bauru (UNESP campus of Bauru).

References

Atterby, H., Smith, N., Chaudhry, Q., & Stead, D. (2002). Exploiting microbes and plants to clean up pesticide contaminated environments. *Pesticide Outlook*, *13*(1), 9–13. DOI: https://doi.org/10.1039/b200937b

Baikousi, M., Georgiou, Y., Daikopoulos, C., Bourlinos, A. B., Filip, J., Zbořil, R., … Karakassides, M. A. (2015). Synthesis and characterization of robust zero valent iron/mesoporous carbon composites and their applications in arsenic removal. *Carbon*, *93*, 636–647. DOI: https://doi.org/10.1016/j.carbon.2015.05.081

Beyer, A., & Biziuk, M. (2009). Environmental fate and global distribution of polychlorinated biphenyls. In D. Whitacre (Ed.), *Reviews of environmental contamination and toxicology* (Vol. 201). Boston, MA: Springer. DOI: https://doi.org/10.1007/978-1-4419-0032-6_5

Cong, L., Guo, J., Liu, J., Shi, H., & Wang, M. (2015). Rapid degradation of endosulfan by zero-valent zinc in water and soil. *Journal of Environmental Management*, *150*, 451–455. DOI: https://doi.org/10.1016/j.jenvman.2014.12.028

Côrtes, P. L., Alves Filho, A. P., Ruiz, M. S., & Teixeira, C. E. (2011). A deposição de resíduos industriais organoclorados no litoral do estado de São Paulo: um estudo de caso. *Review of Administration and Innovation*, *8*(2). DOI: https://doi.org/10.5773/rai.v8i2.700

Cundy, A. B., Hopkinson, L., & Whitby, R. L. D. (2008). Use of iron-based technologies in contaminated land and groundwater remediation: A review. *Science of The Total Environment*, *400*(1), 42–51. DOI: https://doi.org/10.1016/j.scitotenv.2008.07.002

Galassi, S., Viganò, L., & Sanna, M. (1996). Bioconcentration of organochlorine pesticides in rainbow trout caged in the River Po. *Chemosphere*, *32*(9), 1729–1739. DOI: https://doi.org/10.1016/0045-6535(96)00090-2

Huggins, M. L. (1945). Theory of X-ray Diffraction in Crystals (Zachariasen, William H.). *Journal of Chemical Education*, *22*(7). DOI: https://doi.org/10.1021/ed022p364.1

Kamat, P. V, & Meisel, D. (2003). Nanoscience opportunities in environmental remediation. *Comptes Rendus Chimie*, *6*(8), 999–1007. DOI: https://doi.org/10.1016/j.crci.2003.06.005

Li, X., Elliott, D. W., & Zhang, W. (2006). Zero-Valent Iron Nanoparticles for Abatement of Environmental Pollutants: Materials and Engineering Aspects. *Critical Reviews in Solid State and Materials Sciences*, *31*(4), 111–122. DOI: https://doi.org/10.1080/10408430601057611

Litchfield, C. (2005). Thirty Years and Counting: Bioremediation in Its Prime? *BioScience*, *55*(3), 273–279. DOI: https://doi.org/10.1641/0006-3568(2005)055[0273:TYACBI]2.0.CO;2

Mamani, J. B., Gamarra, L. F., & Brito, G. E. S. (2014). Synthesis and characterization of Fe3O4 nanoparticles with perspectives in biomedical applications. *Materials Research*, *17*(3), 542–549. DOI: https://doi.org/10.1590/S1516-14392014005000050

Nie, X., Esopi, M. R., Janik, M. J., & Asthagiri, A. (2013). Selectivity of CO_2 reduction on copper electrodes: the role of the kinetics of elementary steps. *Angewandte Chemie International Edition*, *52*(9), 2459-2462. DOI: https://doi.org/10.1002/anie.201208320

Srivastava, A., Srivastava, N., & Srivastava, K. (2023). Cu(II) catalyzed oxidation of L-phenylalanine by hexacyanoferrate(III) in cationic micellar medium. *South African Journal of Chemistry*, *77*, 143-149. DOI: https://doi.org/10.17159/0379-4350/2023/v77a18

Sun, Y. P., Li, X., Cao, J., Zhang, W., & Wang, H. P. (2006). Characterization of zero-valent iron nanoparticles. *Advances in Colloid and Interface Science*, *120*(1), 47-56. DOI: https://doi.org/10.1016/j.cis.2006.03.001

Sun, Y. P., Li, X. Q., Zhang, W. X., & Wang, H. P. (2007). A method for the preparation of stable dispersion of zero-valent iron nanoparticles. *Colloids and Surfaces A: Physicochemical and Engineering Aspects*, *308*(1), 60–66. DOI: https://doi.org/10.1016/j.colsurfa.2007.05.029

Taha, M. R., & Ibrahim, A. H. (2014). Characterization of nano zero-valent iron (nZVI) and its application in sono-Fenton process to remove COD in palm oil mill effluent. *Journal of Environmental Chemical Engineering*, *2*(1), 1–8. DOI: https://doi.org/10.1016/j.jece.2013.11.021

Terry, N., & Bañuelos, G. (2020). *Phytoremediation of contaminated soil and water* (1. ed.). CRC Press. DOI: https://doi.org/10.1201/9780367803148

Wang, C. B., & Zhang, W. (1997). Synthesizing Nanoscale Iron Particles for Rapid and Complete Dechlorination of TCE and PCBs. *Environmental Science & Technology*, *31*(7), 2154-2156. DOI: https://doi.org/10.1021/es970039c

Xi, Y., Mallavarapu, M., & Naidu, R. (2010). Reduction and adsorption of Pb2+ in aqueous solution by nano-zero-valent iron—A SEM, TEM and XPS study. *Materials Research Bulletin*, *45*(10), 1361-1367. DOI: https://doi.org/10.1016/j.materresbull.2010.06.046

Yin, W., Fan, Z., Zheng, J., Yin, J., Zhang, M., Sheng, X., … Lin, Y. (2012). Characteristics of strike-slip inversion structures of the Karatau fault and their petroleum geological significances in the South Turgay Basin, Kazakhstan. *Petroleum Science*, *9*(4), 444–454. DOI: https://doi.org/10.1007/s12182-012-0228-3

Zhang, W. (2003). Nanoscale iron particles for environmental remediation: an overview. *Journal of Nanoparticle Research*, *5*(3), 323–332. DOI: https://doi.org/10.1023/A:1025520116015

Zhang, W., Nazarian, S., Wang, M., & Cranford, S. W. (2018). Hit or miss: sensor design via scaled collision theory. *Journal of Engineering Mechanics*, *144*(9). DOI: https://doi.org/10.1061/(ASCE)EM.1943-7889.0001487